Aerosol and Air Quality Research, 11: 791–801, 2011

ISSN: 1680-8584 print / 2071-1409 online
doi: 10.4209/aaqr.2011.07.0103

Aerosol Charging Using Pen-Type UV Lamps

Lin Li, Da-Ren Chen*

Department of Energy, Environmental & Chemical Engineering, Washington University in St. Louis, One Brookings Drive, Box 1180, St. Louis, Missouri 63130, U.S.A.

ABSTRACT

A portable aerosol charger utilizing pen-type Hg lamps was constructed to investigate the particle charging process under UV irradiation. The charger primarily consisted of a quartz tube surrounded by four pen-type low-pressure Hg lamps and an ion trap located downstream of the quartz tube to remove excessive ions. The performance of the prototype UV charger at 5 L/min flow rate and with four UV lamps turned on using monodisperse silver (Ag) particles with diameters ranging from 7 to 30 nm was evaluated. As expected, the prototype UV charger provided higher particle charging efficiencies than corona-based unipolar chargers for Ag particles. To evaluate the effect of irradiation intensity on particle photocharging, the charging efficiencies and charge distributions for Ag particles ranged from 7 to 30 nm when the prototype was operated at an aerosol flow rate of 5 L/min for the cases of one, two, and four lamps turned on. The UV charging model with the photoemission based on the Fowler-Nordheim law was further applied to predict the charging performance of the UV charger at different operational conditions.

Keywords: Nanoparticle charging; UV charger; UV irradiation intensity.

INTRODUCTION

Aerosol charging is of importance in aerosol sciences and technology because electrically charged particles are often required in aerosol applications, such as aerosol characterization, particle detection, and control technology (Burtscher, 1992; Mohr *et al*., 1993; Seto *et al*., 1995; Mohr *et al*., 1996; Shimada *et al*., 1997; Chen *et al*., 1998; Jung and Kittelson, 2005). Aerosol charging based on unipolar ion diffusion has been dominantly utilized for particles in the nanometer size range. However, the extrinsic charging efficiency of existing unipolar chargers significantly decreases as the particle size reduces, especially for particles with diameters of less than 20 nm (Chen and Pui, 1999).

To further improve the efficiency of charging nanoparticles, researchers have used direct irradiation methods such as Ultraviolet (UV) (Burtscher *et al*., 1982; Jung *et al*., 1988; Kogelschatz, 1992; Matter *et al*., 1995; Mohr *et al*., 1996; Mohr and Burtscher, 1997; Maisels *et al*., 2003; Hontañón and Kruis, 2008) and soft x-ray irradiation for nanoparticle charging (Kulkarni *et al*., 2002, Shimada *et al*., 2002; Han *et al*., 2003; Jiang *et al*., 2007a). Under UV exposure, electrons can be emitted from the particle surface once irradiated, and irradiated particles thus become positively charged if the incident photon energy exceeds the particle material work function. In soft-X-ray irradiation, gas molecules can be further ionized in addition to direct photoionization because of the high incident photon energy (~10^3 eV). As a result, diffusion charging rates are enhanced in soft-X-ray irradiation when compared to UV irradiation (~5 eV). However, the high cost and limited lifetime of soft X-ray light sources makes them difficult to use.

Schmidt-Ott and Siegmann (1978) investigated photoemission from small particles suspended in a gas upon the irradiation of UV light. Two different UV light sources were used later in research related to aerosol charging: low-pressure mercury lamps (Burtscher *et al*., 1982; Jung *et al*., 1988) and excimer lamps (Kogelschatz, 1992; Maisels *et al*., 2003). The Hg lamp used in Burtscher's charger was bulky, and the charging efficiency was very low (about 12% for 10 nm Ag particles). Jung's charger consisted of a quartz tube (diameter: 8 cm, length 30: cm) with two metallic grids separately laid along the inner wall of the tube. The inner grid was on the electrical ground, and the outer one was on a DC voltage. Jung's charger with a more complex design achieved high charging efficiency (about 90% for 10 nm Ag particles), resulting from the reduction by reattachment of negative ions to the positively charged particles. Excimer lamps usually have larger photon energy and consequently provide higher particle charging efficiency. Using the apparatus developed by Kogelschatz (1992), Mohr *et al*. (1996) obtained an average charge of up to 25 elementary units for diesel particles with a diameter of 100 nm. Furthermore, Mohr and Burtscher

* Corresponding author. Tel.: 1-314-935-7924;
Fax: 1-314-935-5456
E-mail address: Chen@seas.wustl.edu

(1997) observed a reduction of charging efficiency when the particle concentration was in the range of 10^5–10^6 #/cm^3, and the residence time of the ions in the aerosol exceeded a few tens of milliseconds. Hontañón and Kruis (2008) demonstrated the feasibility of UV photoionization for singly unipolar-charged nanoparticles at flow rates up to 100 L/min using a UV-charger consisting of a quartz tube (diameter: 1.6 cm, length: 40 cm) surrounded by three Xe excimer lamps with a wavelength of 172 nm. For monodisperse particles from 5 to 25 nm and at a numerical concentration between 10^4 and 10^5 #/cm^3, the output aerosol concentration of the above UV charger was better than that of the radioactive ionizer (Kr^{85}) when an increased carrier gas flow rate was used. However, excimer lamps are usually much more expensive than Hg lamps, which may limit their use in general aerosol charging applications.

In this study, a UV charger using pen-type Hg lamps was constructed to investigate the aerosol photocharging process by measuring both the charging efficiencies and charge distributions of particles. The charger featured simple construction and portable size. We used DMA-classified silver (Ag) with diameters ranging from 7 to 30 nm as test particles and investigated the effect of light intensity on particle photocharging by varying the number of lamps used in the charger. Finally, the existing UV charging model based on the Fowler-Nordheim equation (Fowler, 1931) was applied to predict the charging performance of the studied UV charger, and it was verified by comparing the results with experimental data.

EXPERIMENTAL SETUP AND PROCEDURES

Description of the Studied UV Charger and Experimental Evaluation

Fig. 1 shows the schematic diagram of the investigated UV aerosol charger. The basic configuration of the prototype was a quartz tube about 7 in. long which was surrounded by four low pressure Hg lamps with a 6 in. lighted length (UVP model 96-0004-7). We used a cylindrical aluminum case having an aerosol inlet and outlet at the ends to enclose the quartz tube and lamps in order to prevent operators from being exposed to UV light and for the purpose of transporting aerosol through the quartz tube without contact with the lamps. We also designed an ion trap at the quartz tube exit to minimize the recombination of positively charged particles and negative ions. In general, the voltage required to remove ions is a function of the flow rate through the ion trap: the higher aerosol flow rate, the higher ion-trap voltage. In this study, the ion trap voltage was set at –10 V.

The experiments to characterize the performance of the UV aerosol charger included the measurements of the charging efficiency and charge distribution of particles existing from the charger. With regard to the particle charging efficiency, both intrinsic and extrinsic efficiencies are key parameters for the performance evaluation of an aerosol charger. In this study, we defined the intrinsic charging efficiency as the percentage of entering neutral particles acquiring electrical charges in the charger disregarding their final fates (i.e., either exiting or lost in the charger), and the extrinsic charging efficiency was defined as the percentage of entering neutral particles which acquired electrical charges in the charger and made their exit. The difference between the intrinsic and extrinsic particle charging efficiencies thus represents the loss of charged particles in the charger (Qi *et al*., 2007).

Monodisperse Aerosol Generation

Included in Fig. 2(a) is the aerosol generation system used to produce monodipserse test aerosols for this investigation. Polydisperse Ag particles were generated by the evaporation-and-condensation method (Scheibel and Porstendörfer, 1983). Using the above method, Ag fine powder was placed in a ceramic boat located in a high-temperature tube furnace (Lindberg/Blue Model CC58114A-1). Nitrogen at a flow rate of 1.5 L/min was used as the vapor carrier gas in the tube furnace. A needle valve and a laminar flow meter regulated and monitored the flow rate of the carrier gas prior to its introduction into the ceramic tube used in the furnace. At a high temperature, the Ag powder in the ceramic boat was evaporated, and its vapor was carried out of the furnace by the nitrogen flow. At the exit of the

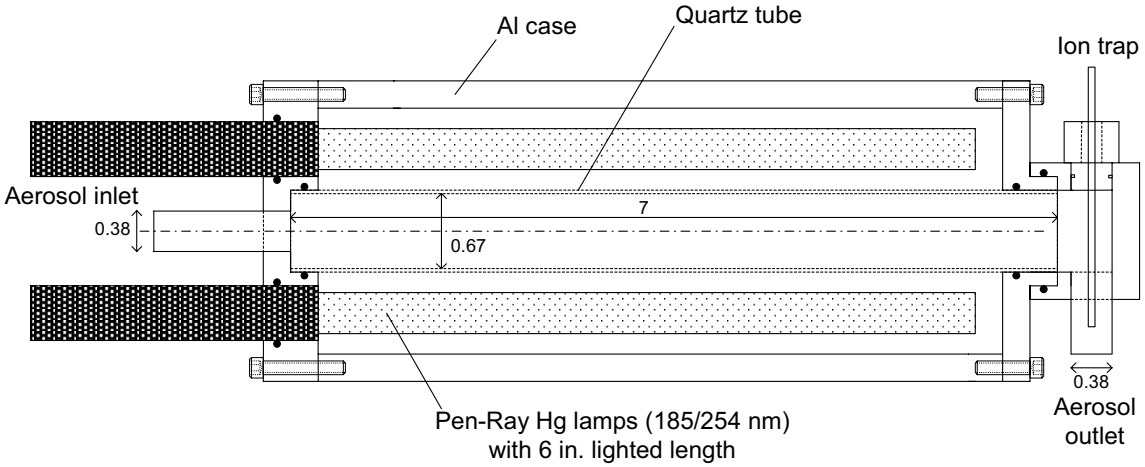

Fig. 1. Schematic diagram of the studied UV charger (Unit: inch).

furnace tube, polydisperse nanoparticles were formed by mixing the hot, vapor-enriched carrier gas with particle-free air at room temperature. Downstream of the polydisperse aerosol generation system, a differential mobility analyzer (DMA, TSI Model 3085) was used to classify monodisperse particles with the desired sizes (Liu and Pui, 1974). Prior to the DMA classification, a Kr^{85} radioactive particle charger was induced to achieve a well-defined charge distribution for input polydisperse particles (Knutson and Whitby, 1975). The DMA at the aerosol flow rate of 1.5 L/min and sheath flow rate of 15.0 L/min was also operated. To obtain electrically neutral particles for the charger evaluation, DMA-classified particles through a Po^{210} radioactive particle neutralizer and an electrostatic condenser at high voltage (around 4 KV) were further directed to remove charged particles. For the charger evaluation, monodisperse Ag particles with diameters ranging from 7 to 30 nm were produced with the generation technique described above.

Experimental Setup

Shown in Fig. 2(b) is the experimental setup for the performance evaluation of the UV charger. For the particle charging efficiency measurement, the charged fraction of the particles exiting the UV charger were measured by passing the aerosol stream through a second electrostatic condenser to remove all charged particles, and then the particles were directed to an ultrafine condensation particle counter (UCPC, TSI model 3025A) to count the numeric concentration of neutral particles in the stream. In the measurement, the UCPC vacuum pump was operated at high flow mode (i.e., 1.5 L/min), and the house vacuum controlled the aerosol flow rate through the UV charger. A laminar flow meter and a needle valve in the gas line were set to control the flow rate of the vacuum source.

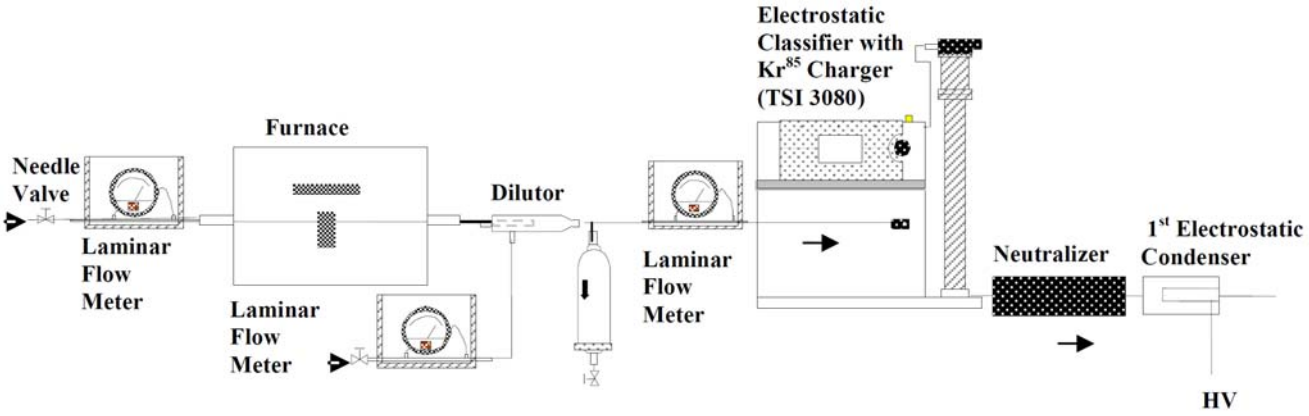

Fig. 2(a). Aerosol generation system to produce neutral monodisperse test particles.

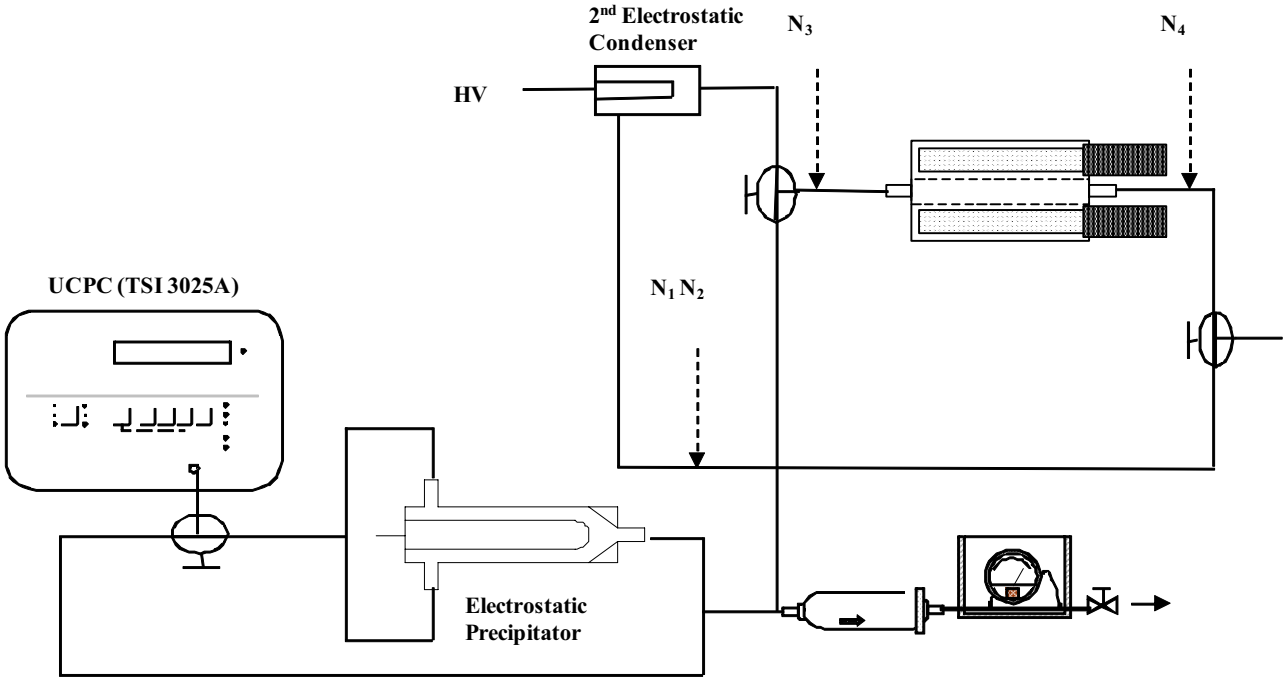

Fig. 2(b). Experimental setup for the performance evaluation of the UV charger.

The intrinsic particle charging efficiency was then calculated using the method of Romay and Pui (1992):

$$\eta_{in} = 1 - \frac{N_1}{N_2}, \quad (1)$$

where η_{in} is the intrinsic charging efficiency, and N_1 and N_2 are the particle number concentrations measured downstream of the second electrostatic condenser with applied high voltage turned on and off, respectively. The extrinsic particle charging efficiency was evaluated using the method described by Chen and Pui (1999):

$$\eta_{ex} = \frac{N_3 - N_1 / P_{ec}}{N_4}, \quad (2)$$

where η_{ex} is the extrinsic charging efficiency; N_3 is the number concentration of particles exiting the UV charger when it is turned on; N_4 is the number concentration of particles entering the UV charger, and P_{ec} is the penetration of neutral particles through the second electrostatic condenser.

This study further characterized particle charge distribution after particles passed through the UV charger. The particle generation systems for this part of the experiment were the same as those described previously. Due to the high charge level on particles, it is possible that particles with n and n + 1 charges all fell into the same size channel when using SMPS to measure charge distribution. Thus, it was difficult to use the TDMA technique to directly measure the charge distribution of particles with high resolution. Instead, we used an electrostatic precipitator technique in this study for the charge distribution measurement (Adachi *et al*., 1991; Forsyth *et al*., 1998). The characteristic curve of charge particle penetration through an electrostatic precipitator can be, in general, expressed as

$$P = 1 - \eta_c = 1 - KZ_p \mathrm{V}, \quad (3)$$

where K is a function of precipitator dimension; V is the applied voltage on the precipitator, and Z_p is the particle electrical mobility with the expression $Z_{p,n} = n_p e C_c / 3\pi\mu d_p$, in which n_p is the particle electrical charge; C_c is the Cunningham correction factor, and μ is the gas viscosity. The performance of the used electrostatic precipitator was calibrated using monodisperse, charged particles of various sizes, and the characteristic curve was achieved from experimental data prior to this study.

Assuming the total charge fraction is equal to 1, $\sum F_n = 1$ (where F_n is the fraction of particles with n charges), the particle penetration $P(d_p, V_m)$ with diameter d_p at rod voltage V_m, was calculated as $P(d_p, V_m) = 1 - KV_m \sum F_n Z_{p,n}$.

In the electrostatic precipitator technique, the penetration of charged particles through the precipitator at different applied voltages was measured with a UCPC. The electrical mobility distribution of particles leaving the charger was retrieved by comparing the calculated penetration with collected experimental data using the Bayesian statistic analysis (Ramachandran and Kandlikar, 1996; Hogan *et al*., 2009). The charge distribution of particles was then derived from the electrical mobility distribution of the particles. Note that the derived charge distribution obtained in our study was for particles at the charger exit (i.e., extrinsic particle charge distribution), not in the UV irradiation zone (i.e., intrinsic charge distribution).

PHOTOCHARGING MODEL

Previous works have addressed modeling of aerosol charging by simultaneous photoionization and gaseous ion diffusion (Maisels *et al*. 2002; Jiang *et al*. 2007a; Hontañón and Kruis, 2008). The evolution with time of the concentration of ions and particles in a gas flow under the exposure of UV radiation is governed by the population balance equations:

$$\frac{dN_i}{dt} = \sum_{R_p} \sum_{q} [\alpha^{q-1 \to q} - \beta^{q+1 \to q} N_i] N_{R_p,q} - \Delta_i, \quad (4)$$

$$\frac{dN_{R_p,q}}{dt} = [\alpha^{q-1 \to q} N_{R_p,q-1} - \alpha^{q \to q+1} N_{R_p,q}] + N_i [\beta^{q+1 \to q} N_{R_p,q+1} - \alpha^{q \to q-1} N_{R_p,q}] - \Delta N_{R_p,q}, \quad (5)$$

where N_i is the concentration of negative ions in the gas; $N_{Rp,q}$ is the concentration of particles with the size of R_p; Δ_i is the particle loss to the charger walls; β is the ion-to-particle attachment coefficient, and α is the photo-ionization rate.

The ion-to-particle attachment coefficients are calculated based on the theory of the limiting sphere by Fuchs (1963):

$$\beta = \frac{\pi\theta c_i \delta^2 \exp(-\frac{\phi(\delta)}{kT})}{1 + \frac{\theta c_i \delta^2}{4D_i} \exp(-\frac{\phi(\delta)}{kT}) \int_{\delta}^{\infty} \frac{1}{r^2} \exp(\frac{\phi(r)}{kT}) dr}, \quad (6)$$

where θ is the probability of an ion entering the limiting sphere to collide and transfer its charge to particles; δ is the limiting-sphere radius, which is a function of particle radius and the ion mean free path; c_i and D_i are the mean thermal velocities and the diffusion coefficients of the ion, respectively; $\varphi(r)$ is the potential energy at the distance r from the center of particle; k is the Boltzmann's constant, and T is the temperature of the system.

The photo-ionization rate α is the photoelectric yield coefficient (the photoelectron yield per time for given particles)

$$\alpha = Y(h\upsilon) \frac{I}{h\upsilon} \pi R_p^2, \quad (7)$$

where $Y(h\upsilon)$ denotes the electron yield per incident photon; h is the Planck's constant; υ is the frequency of UV irradiation, and I is the intensity of the radiation. Current models of photoelectric aerosol charging rely on the Fowler-Nordheim law for photoemission from clean surfaces:

$$Y(h\upsilon) = K_c(h\upsilon - \Phi)^m \text{ (Fowler 1931)}, \quad (8)$$

where K_c and m are material-dependent constants, and Φ stands for the photothreshold for metallic spheres, with the form

$$\Phi = \Phi_\infty + \frac{e^2}{4\pi\varepsilon_0}\left(\frac{q+1}{R_p} - \frac{5}{8R_p}\right) \text{ (Wood 1981)}, \quad (9)$$

where Φ_∞ denotes the work function, i.e., the photo-threshold for an infinite planar surface, which is a characteristic of the material, and ε_0 and e are the permeability of the vacuum and elementary charge, respectively. The Fowler-Nordheim law has been successfully used to predict the photoemission yield of a variety of metallic particles, PbS, and SnO with $m = 2$ (Schleicher *et al*., 1993; Maisels *et al*., 2003; Hontañón and Kruis, 2008).

After substituting in Eq. (7), the photoionization rate α is then expressed as

$$\alpha = K_c I \frac{\pi R^2}{h\upsilon}\left[h\upsilon - \Phi_\infty - \frac{e^2}{4\pi\varepsilon_0 R}\left(q + \frac{3}{8}\right)\right]^2. \quad (10)$$

This equation shows that, when $h\upsilon > \Phi$, a sphere can be photoionized up to a maximum charge level at which the process saturates. The maximum can be derived from Eq. (10) when photo-ionization rate α is equal to 0:

$$q_{\max} = \frac{4\pi\varepsilon_0}{e^2}(h\upsilon - \Phi_\infty)R - \frac{3}{8}. \quad (11)$$

The limiting aerosol charging case in which the photo-ionization dominates the ion attachment to particles (i.e., $\alpha >> \beta N_i$) is analyzed herein. The ion balance equation is irrelevant in such a case. For simplicity, we assumed the aerosol to be monodisperse and electrically neutral. The wall loss of particles was further assumed to be negligible. Using the birth-and-death theory as proposed by Boisdron and Brock (1970), the particle balance equations can be solved and the result is as follows:

$$N_{R_p,q} = \begin{cases} \exp(-\alpha^{0\to 1}t) & for \quad q = 0 \\ -\sum_{j=0}^{q-1} k_{j,q-1}\frac{\alpha^{q-1\to q}}{\alpha^{j\to j+1} - \alpha^{q\to q+1}}\left[\exp(-\alpha^{j\to j+1}t) - \exp(-\alpha^{q\to q+1}t)\right] & for \quad 0 < q < q_{\max} \end{cases}, \quad (12)$$

with

$$k_{j,q} = \begin{cases} 1 \\ -k_{j,q-1}\frac{\alpha^{q-1\to q}}{\alpha^{j\to j+1} - \alpha^{q\to q+1}} \\ -\sum_{j=0}^{q-1} k_{j,q} \\ 0 \end{cases}, \quad (13)$$

where q is the number of elementary charges on particle, and j and k are the coefficients for calculation.

RESULTS AND DISCUSSION

Charging Efficiency of the UV Charger

Monodisperse Ag particles with a diameter of 10 nm were selected as our initial test aerosol. Fig. 3 shows the intrinsic and extrinsic charging efficiencies of the UV charger at various aerosol flow rates. As expected, the intrinsic charging efficiencies decreased with the increase of aerosol flow rate. The extrinsic charging efficiency

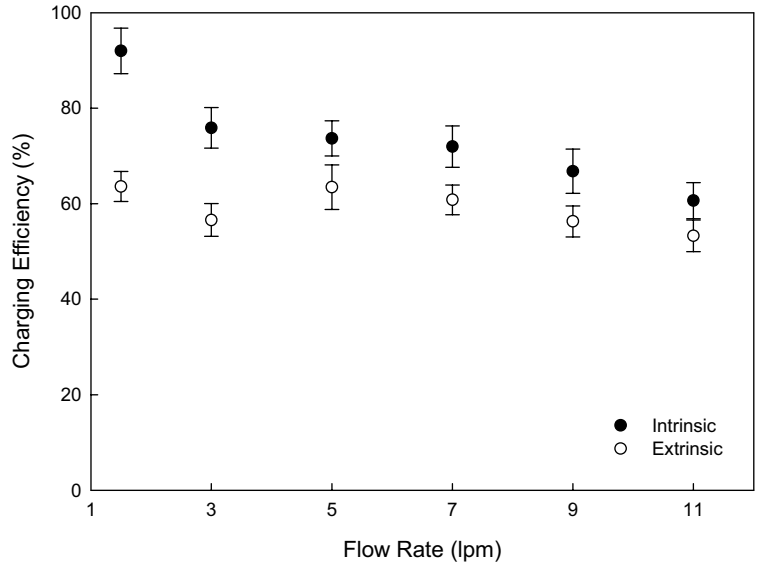

Fig. 3. Intrinsic and extrinsic charging efficiencies of 10 nm Ag particles at different aerosol flow rates.

remained nearly constant below 5 L/min and decreased after further increasing the aerosol flow rate. The maximal extrinsic charging efficiency occurred at around 5 L/min aerosol flow rate. With a lower flow rate, the residence time in the charging zone can be increased, which leads to an increase in intrinsic charging efficiency and the number of particle charges. However, highly charged particles have larger electrical mobility as compared to singly-charged ones of the same size. It was thus expected that highly charged particles would be much more easily deposited in the charger because of the space charge effect resulting from highly charged particles and the electrical attraction due to image force when they moved close to the charger wall. At a low flowrate (i.e., 1.5 L/min), the ion trap may also capture some of highly charged particles having high electrical mobility because particles in nanometer sizes are also easily lost during transportation in the prototype because of the particle diffusion. Operating the prototype at a high aerosol flowrate, resulting in less resident time, should reduce the particle loss. Unfortunately it also reduces the intrinsic charging efficiency of the prototype, resulting in the decrease in extrinsic charging efficiency. To achieve better overall charger performance, we selected a 5 L/min aerosol flowrate for the following tests.

The intrinsic and extrinsic charging efficiencies for Ag particles with diameters ranging from 7 to 30 nm when the UV charger was operated at an aerosol flow rate of 5 L/min with four lamps turned on are shown in Fig. 4. For comparison, we also included the experimental charging efficiencies of Buscher's charger (Buscher *et al*., 1994), the twin Hewitt charger (Kruis and Fissan, 2001), the mixing-type charger (Qi *et al*., 2007), and the charge conditioner (Li *et al*., 2011). For the intrinsic charging efficiency (shown in Fig. 4(a)), the UV charger performed better than both the mixing-type charger and the charge conditioner. The intrinsic charging efficiency was found to be higher than 90% for particles with diameters larger than 15 nm. For the extrinsic charging efficiency (given in Fig. 4(b)), the prototype achieved charging higher than 80% for particles of diameters larger than 15 nm. Over 90% of the charged particles in the studied size range exited the UV charger. Note that, for particles less than 7 nm in diameter, the extrinsic charging efficiency was expected to be reduced because of their high diffusivity and electrical mobility. Further, the UV charger performed better than existing corona-based aerosol chargers. The above observation could be attributed to different aerosol charging mechanisms used in photo- and corona-based chargers and the fast aerosol exiting passage designed in the studied UV charger. In the case of a corona-based charger, the charging performance is a function of the ion-to-particle attachment coefficient, the ion concentration and particle residence time in the device. It is much more difficult for charged particles to get additional charges of the same polarity because of the columbic repulsion force. In the case of UV chargers, the charging is related to photon energy, irradiation intensity and particle work function. Particles get an additional charge when the photon energy is higher than the particle work function.

A DMA connected to an external positive high voltage power supply downstream of the UV charger was used to determine if there were any negative ions or particles in the aerosol stream. The absence of negatively charged particles observed indicated that diffusion charging played a negligible role in altering electrical charges on particles after their leaving the irradiation zone of the studied charger. This observation was attributed to the low ion production in the UV charger because of the low particle concentrations used in our evaluation. Furthermore, the quartz tube was actually heated by the absorption of UV light in the experiment. The temperature of the tube was higher than that of the test aerosol stream. The temperature of the metal case of the prototype was measured at about

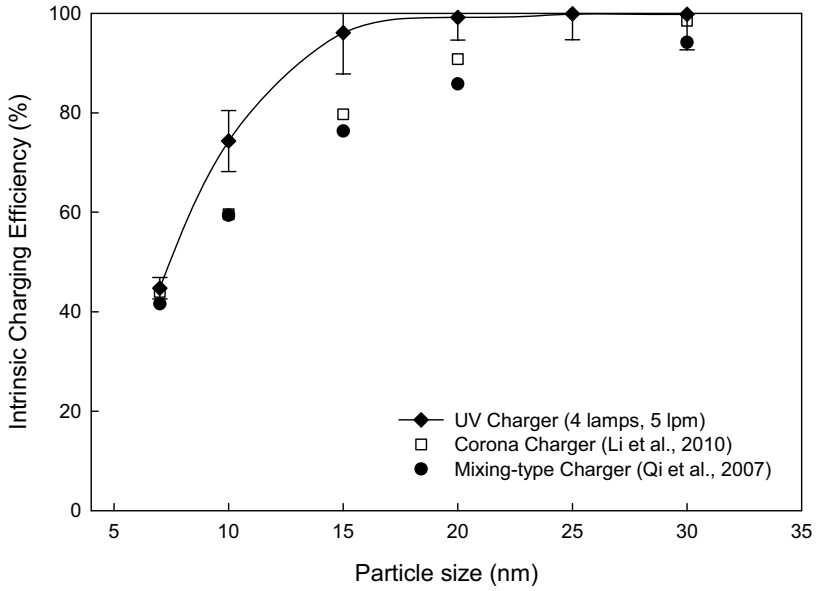

Fig. 4(a). Comparison of intrinsic charging efficiencies among different chargers for Ag particles in the size range from 7 to 30 nm.

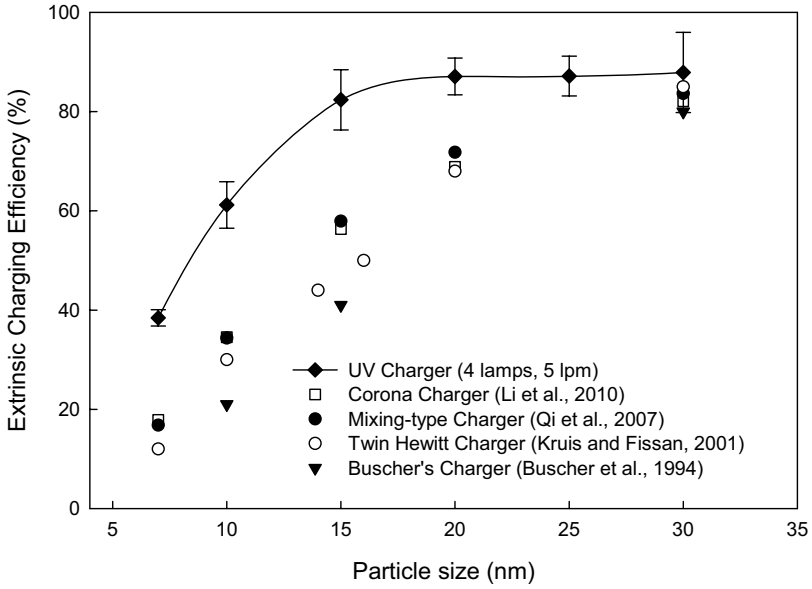

Fig. 4(b). Comparison of extrinsic charging efficiencies among different chargers for Ag particles in the size range from 7 to 30 nm.

50°C. Thermophoretic force resulting from the temperature gradient between aerosol stream and tube wall may have kept particles in the center of the tube. The estimated thermophoretic velocity due to the temperature gradient was three orders of magnitude less than the aerosol velocity. The thermophoretic effect on aerosol behavior in the prototype was thus considered negligible in this study.

Charging Distribution on Particles Exiting the UV Charger

This experiment was performed to measure the charge distribution on particles exiting the UV charger operated at 5 L/min aerosol flow rate with the four UV lamps turned on. Fig. 5 shows the measured charge distributions for Ag particles with diameters from 7 to 25 nm after their passing through the UV charger. The concentrations of test particles were kept at the level of 1×10^3–2×10^4 #/cm^3. Note that the experimental data shown in Fig. 5 are in fact the extrinsic rather than intrinsic charge distribution of the particles. As expected, particles of large sizes exhibited lower work function and larger collision cross-section for photons as compared to ones of smaller sizes, resulting in higher photoionization rate. Thus, because it is easier for large particles to get electrically charged, as a result, the particle charge distributions move towards the regime of high charges as the particle size increases.

Effect of Irradiation Intensity

Fig. 6 shows the intrinsic charging efficiencies for Ag particles of diameters ranging from 7 to 30 nm when the UV charger was operated at an aerosol flow rate of 5 L/min with one, two, or four lamps turned on. In the case of two UV lamps, two diagonal ones were used to get better spatial uniformity of UV irradiation in the charging zone. As a reference, the intrinsic charge efficiencies calculated from the above photocharging model are also plotted in Fig. 6. Table 1 lists the values of the parameters used to calculate particle photoionization rate α in our study. In all these cases, diffusion charging was determined to be negligible because the ratio of the photionization rate to the diffusion charging rate was greater than 100. The calculated curves shown in Fig. 6 represent the analytical solution to best fit the experimental data by varying the combination value of the photoemission constant K_c and the intensity of incident light I, which are often difficult to characterize, and thus are determined empirically (Maisels *et al*., 2002, 2003; Jiang *et al*., 2007a, 2007b; Hontañón and Kruis, 2008). The best-fitted value of K_cI is also given in the legend of the figure. The low-pressure Hg lamps used in our study had light emissions with wavelengths of 185 and 254 nm rated by the vendor. From our study, we concluded that the photocharging process in the studied UV charger was in fact dominated by the irradiation with the wavelength of 185 nm, not 254 nm. When the wavelength was set at 254 nm, the maximum charge level of 15 and 25 nm Ag particles were 3 and 5 charges. However, from Figs. 5(c) and 5(d), the charge status of 15 and 25 nm Ag particles can be seen to be higher than those calculated using a 254 nm wavelength. Thus, the photocharging process in the studied UV charger was dominated by the irradiation with the wavelength of 185 nm. Compared with Jung's result, the charging efficiency of the studied charger was lower. This was probably because of the low irradiation intensity of compact Pen-type UV lamps used. The efficiency of the studied charger could be further improved by including more lamps. Note that a UV charging model was also utilized and tuned in our study to predict the performance of the studied charger. The developed charging model can be used to predict the performance of UV chargers for particles of different particle sizes. Such modeling work was not included in the Jung's study.

For a given irradiation condition, a constant value of K_cI enabled us to get a good fit to the corresponding intrinsic

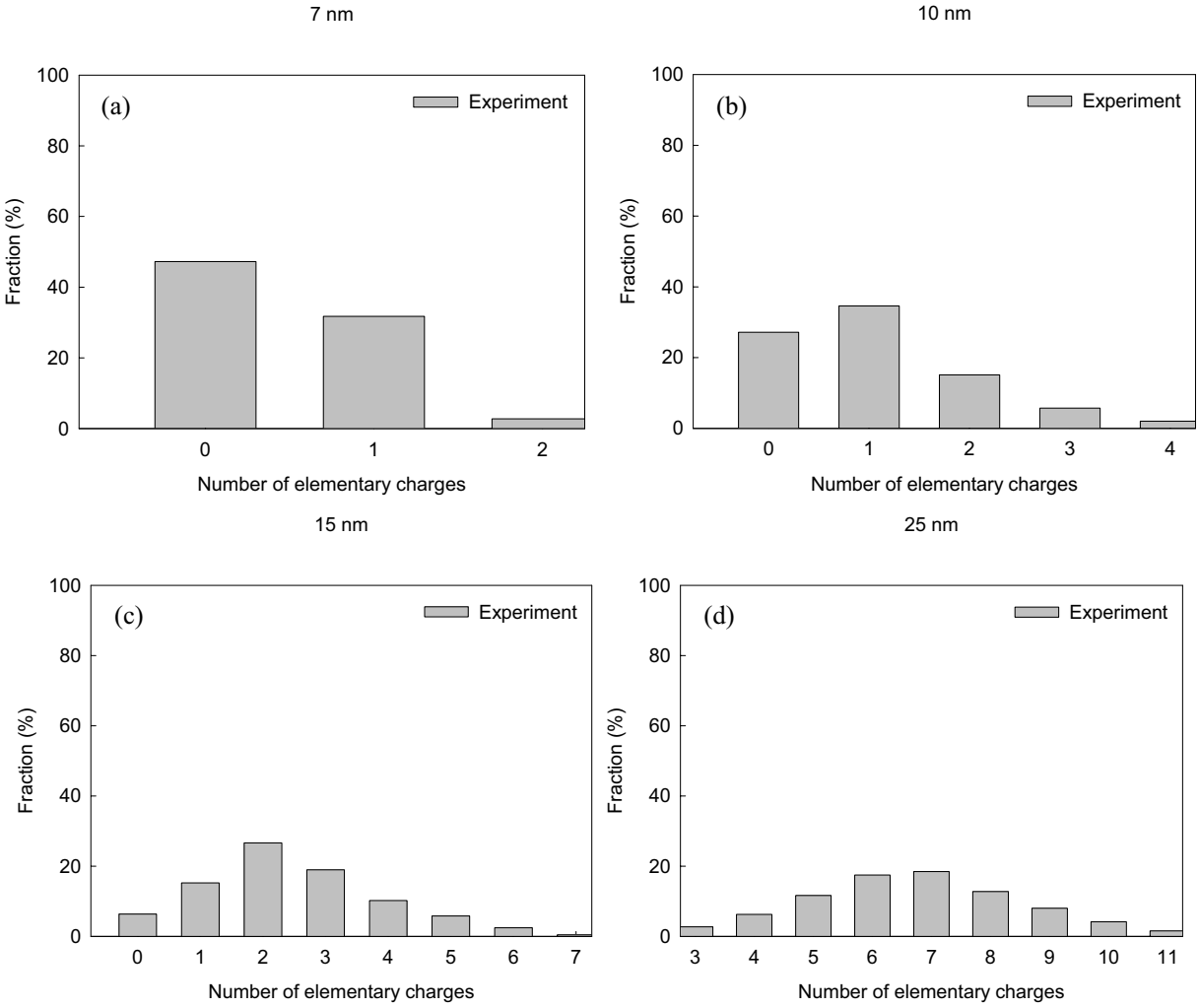

Fig. 5. Extrinsic charge distributions of Ag particles with diameter from 7 to 25 nm at an aerosol flow rate of 5 L/min with four UV lamps.

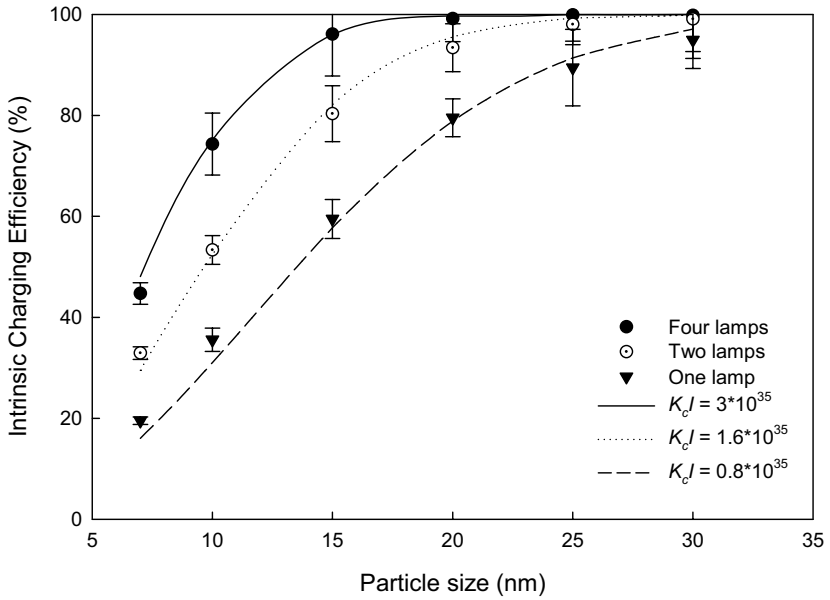

Fig. 6. Comparison of intrinsic charging efficiencies of the UV charger for Ag particles in the size range from 7 to 30 nm at an aerosol flow rate of 5 L/min with one, two, and four UV lamps.

charging efficiency measured for test particles of sizes between 7 and 30 nm. We thus concluded that no dependence of the photoemission constant K_c on the particle size was observed for Ag particles in the tested size range. The aerosol photocharging model used assumed the light intensity in the irradiation zone of the UV charger to be uniform. The discrepancy between the experimental and calculated efficiency data might be because of the spatial non-uniformity of the light intensity in the irradiation zone. Further, the ratio of the K_cI values at the three light intensity conditions was 3.75:2:1, which was close to the number ratio of UV lamps (i.e., 4:2:1) used in the corresponding cases. It is thus evident that the photoionization rate α was proportional to the light intensity I.

Fig. 7 shows the charge distributions of Ag particles with a diameter of 15 nm and at a concentration of approximately 2×10^4 #/cm^3 under the irradiation of various numbers of UV lamps. As a reference, Fig. 7 also gives the intrinsic charge distributions calculated by the photocharging model. The best-fitted K_cI values obtained from the intrinsic charging efficiency data were used in this calculation of particle charge distribution. As expected, particle charge distributions moved towards the status of a single charge with the decrease in light intensity. A reasonable agreement was obtained between the experimental and calculated charge distributions in our study. The discrepancy between measured and calculated charge distributions can be attributed to the loss of charged particles in the charger and the non-uniform light intensity in the irradiation zone.

CONCLUSIONS

Aerosol photocharging was investigated through a simple UV charger with pen-type UV lamps. The studied UV charger consisted of a quartz tube about 7 in. long as the aerosol irradiation zone, four low-pressure Hg lamps located around the quartz tube, and an outer cylindrical aluminum case with aerosol inlet at one end and an outlet at the

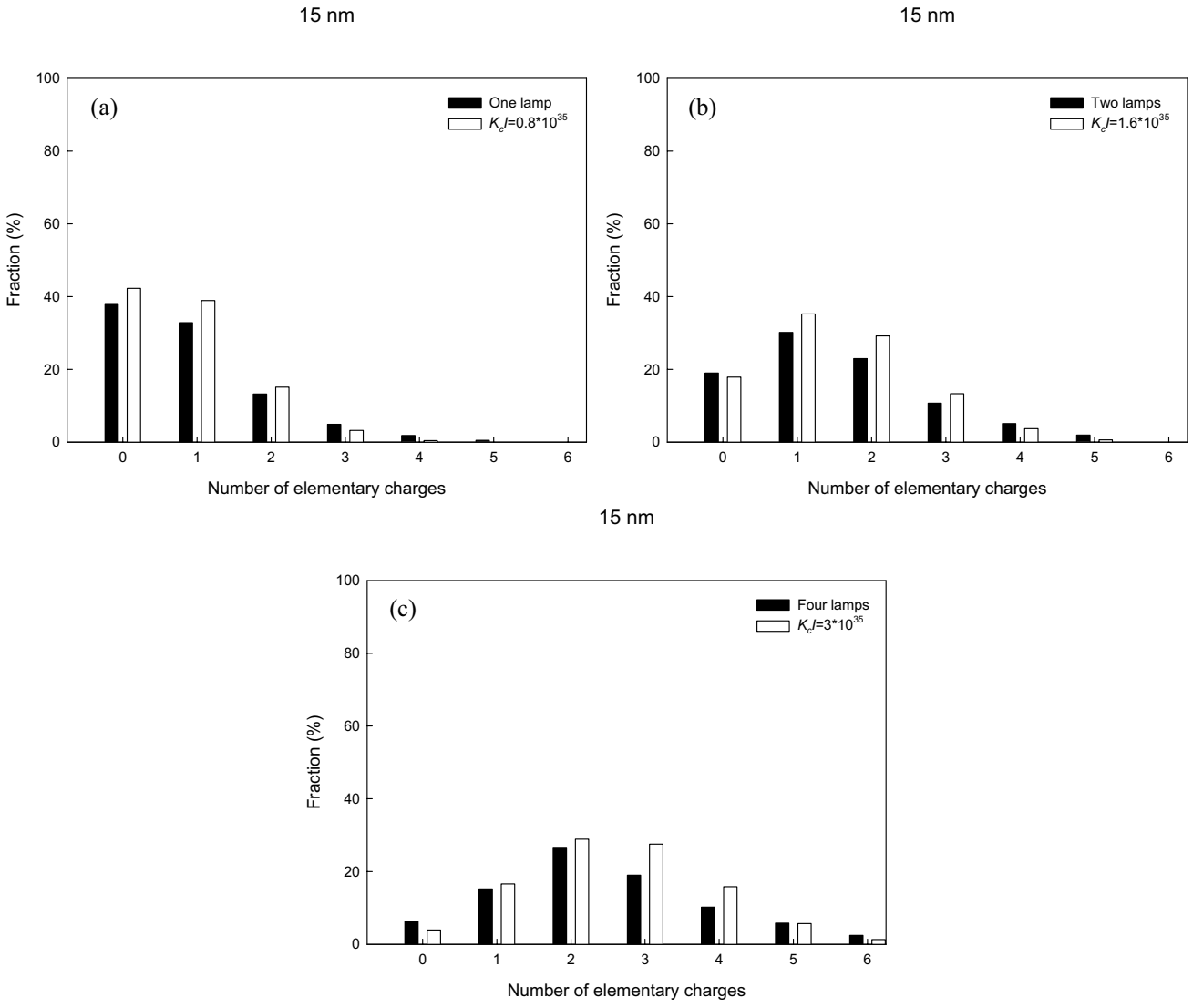

Fig. 7. Comparison of extrinsic charge distributions of 15 nm Ag particles at the concentration of approximately 2×10^4 #/cm^3 with one, two, and four UV lamps.

other end. The charger also had an ion trap section at the exit of the quartz tube to remove free ions.

The performance of the UV charger was experimentally evaluated operating at a 5 L/min flow rate and with four UV lamps turned on using monodisperse Ag with diameters from 7 to 30 nm. Both extrinsic and extrinsic charging efficiencies of the UV charger were characterized and compared with existing corona-based chargers. The studied UV charger provided higher extrinsic charging efficiencies than corona-based unipolar chargers for Ag particles. The extrinsic charging efficiency of the prototype was found to be higher than 80% for particles of diameters larger than 15 nm. Charge distributions of monodisperse Ag particles at the exit of the UV charger, operating at a 5 L/min aerosol flow rate and with four UV lamps turned on, were measured by the electrostatic precipitation technique.

To evaluate the effect of irradiation intensity on particle photocharging, the charging efficiencies and charge distributions were measured for Ag particles with sizes from 7 to 30 nm at an aerosol flow rate of 5 L/min, with one, two, or four lamps turned on. This study used the UV charging model with the photoemission following the Fowler-Nordheim law to obtain the K_cI values at various operational conditions by best fitting to the measured intrinsic charging efficiency. The same K_cI values obtained above were then used in the charging model to calculate the charge distribution of particles. The study achieved reasonable agreement between calculated and measured charge distributions of particles.

REFERENCES

Adachi, M., Liu, B.Y.H. and Piu, D.Y.H. (1991). Development of an Automatic System for Measuring Particle Charge and Size Distributions in a Clean Room. *Part. Part. Syst. Char.* 8: 200–208.

Boisdron, K. and Brock, J.R. (1970). On the Stochastic Nature of the Acquisition of Electrical Charge and Radioactivity by Aerosol Particles. *Atmos. Environ.* 4: 35–50.

Burtscher, H. (1992). Measurement and Characterization of Combustion Aerosols with Special Consideration of Photoelectric Charging and Charging by Flame Ions. *J. Aerosol Sci.* 23: 549–595.

Burtscher, H., Scherrer, L., Siegmann, H.C., Schmidt-Ott, A. and Federer, B.J. (1982). Probing Aerosol by Photoelectric Charging. *J. Appl. Phys.* 53: 3787–3791.

Buscher, P., Schmidt-Ott A. and Wiedensohler, A. (1994). Performance of a Unipolar 'Square Wave' Diffusion Charger with Variable nt-product. *J. Aerosol Sci.* 25: 651–663.

Chen D.R. and Pui, D.Y.H. (1999). A High Efficiency, High Throughput Unipolar Aerosol Charger for Nanoparticles. *J. Nanopart. Res.* 1: 115–126.

Chen, D.R., Pui, D.Y.H., Hummes, D., Fissan, H., Quant, F.R. and Sem G.J. (1998). Design and Evaluation of a Nanometer Aerosol Differential Mobility Analyzer (Nano-DMA). *J. Aerosol Sci.* 29: 497–509.

Forsyth, B., Liu, B.Y.H. and Romay, F.J. (1998). Particle Charge Distribution Measurement for Commonly Generated Laboratory Aerosols. *Aerosol Sci. Technol.* 28: 489–501.

Fowler, R.H. (1931). The Analysis of Photoelectric Sensitivity Curves for Clean Metals at Various Temperatures. *Phys. Rev.* 38: 45–56.

Fuchs, N.A. (1963). On the Stationary Charge Distribution on Aerosol Particles in Bipolar Ionic Atmosphere. *Pure Appl. Geophys.* 56: 185–193.

Han, B., Shimada, M., Choi, M. and Okuyama K. (2003). Unipolar Charging of Nanosized Aerosol Particles Using Soft X-ray Photoionization. *Aerosol Sci. Technol. 3*7: 330–341.

Hogan, C.J., Li, L., Biswas, P. and Chen, D.R. (2009). Estimating Aerosol Particle Charging Parameters Using a Bayesian Inversion Technique. *J. Aerosol Sci.* 40: 295–306.

Hontañón, E. and Kruis, F. (2008). Single Charging of Nanoparticles by UV Photoionization at High Flow Rates. *Aerosol Sci. Technol.* 42: 310–323.

Jiang, J., Hogan, C.J. and Biswas, P. (2007a). Aerosol Charging and Capture in the Nanoparticle Size Range (6–15 nm) by Direct Photoionization and Diffusion Mechanisms. *J. Appl. Phys.* 102: 034904.

Jiang, J., Lee, M.H. and Biswas, P. (2007b). Model for Nanoparticle Charging by Diffusion, Direct Photoionization and Thermoionization Mechanisms. *J. Electrostat.* 65: 209–220.

Jung, H. and Kittelson, D.B. (2005). Characterization of Aerosol Surface Instruments in Transition Regime. *Aerosol Sci. Technol.* 39: 902–911.

Jung, Th., Burtscher, H. and Schmidt-Ott, A. (1988). Multiple Charging of Ultrafine Aerosol Particles by Aerosol Photoemission (APE). *J. Aerosol Sci.* 19: 485–490.

Knutson, E.O. and Whitby, K.T. (1975). Aerosol Classification by Electric Mobility: Apparatus, Theory, and Applications. *J. Aerosol Sci.* 6: 443–421.

Kogelschatz, U. (1992). Silent-discharge Driven Excimer UV Sources and Their Applications. *Appl. Surf. Sci.* 54: 410–423.

Kruis, F.E. and Fissan, H. (2001). Nanoparticle Charging in a Twin Hewitt Charger. *J. Nanopart. Res.* 3: 39–50.

Kulkarni, P., Namiki, N., Otani, Y. and Biswas, P. (2002). Charging of Particles in Unipolar Coronas Irradiated by In-situ Soft X-rays: Enhancement of Capture Efficiency of Ultrafine Particles. *J. Aerosol Sci.* 33: 1279–1296.

Li, L. and Chen D R. (2011). Performance Study of a DC-Corona-based Particle Charger for Charge Conditioning. *Aerosol Sci. Technol.* 42: 87–99.

Liu, B.Y.H. and Piu, D.Y.H. (1974). A Submicrion Aerosol Standard and the Primary, Absolute Calibration of the Condensation Nuclei Counter. *J. Colloid Interface Sci.* 47: 156–171.

Maisels, A., Jordan, F. and Fissan, H. (2002). Dynamics of the Aerosol Particle Photocharging Process. *J. Appl. Phys.* 91: 3377–3383.

Maisels, A., Jordan, F. and Fissan, H. (2003). On the Effect of Charge Recombination on the Aerosol Charge Distribution in Photocharging Systems. *J. Aerosol Sci.* 34: 117–132.

Matter, D., Mohr, M., Fendel, W., Schmidt-Ott, A. and Burtscher H. (1995). Multiple Wavelength Aerosol Photoemission by Excimer Lamps. *J. Aerosol Sci.* 26: 1101–1115.

Mohr M., Kwetkus, B.A. and Burtscher, H. (1993). Improvement of Electrostatic Precitpitation by UV-charging of Submicron Particles. *J. Aerosol Sci.* 24: S247–S248.

Mohr, M. and Burtscher, H. (1997). Photoelectric Aerosol Charging at High Particle Concentrations. *J. Aerosol Sci.* 28: 613–621.

Mohr, M., Matter, D. and Burtscher, H. (1996). Efficient Multiple Charging of Diesel Particles by Photoemission. *Aerosol Sci. Technol.* 24: 14–20.

Qi, C., Chen, D.R. and Pui, D.Y.H. (2007). Experimental Study of a New Corona-based Unipolar Aerosol Charger. *J. Aerosol Sci.* 38: 775–792.

Ramachandran, G. and Kandlikar, M. (1996). Bayesian Analysis for Inversion of Aerosol Size Distribution Data. *J. Aerosol Sci.* 27: 1099–1112.

Romay, F.J. and Pui, D.Y.H. (1992). On the Combination Coefficient of Positive Ions with Ultrafine Neutral Particles in the Transition and Free-molecule Regime. *Aerosol Sci. Technol.* 17: 134–147.

Scheibel, H.G. and Porstendörfer, J. (1983). Generation of Monodisperse Ag- and NaCl-aerosol with Particle Diameters between 2 and 300 nm. *J. Aerosol Sci.* 14: 113–126.

Schleicher, B., Burtscher, H. and Siegmann, H.C. (1993). Photoelectric Quantum Yield of Nanometer Metal Particles. *Appl. Phys. Lett.* 63: 1191–1193.

Schmidt-Ott, A. and Siegmann, H.C. (1978). Photoelectron Emission from Small Particles Suspended in Air. *Appl. Phys. Lett.* 32: 710–713.

Seto, T., Okuyama, K., Inoue, Y., Yokoyama, S., Kurose, S., Hirose, M. and Fujii, T. (1995). Fine Particulate Contaminant Control by the UV/Photoelectron Method under a Low Pressure Condition. *Rev. Sci. Instrum.* 66: 5348–5351.

Shimada, M., Cho, S.J., Okuyama, K., Tamura, T., Adachi, M. and Fujii, T. (1997). Removal of Airborne Particles by a Tubular Particle Removal Device Using UV/Photoelectron Method. *J. Aerosol Sci.* 28: 649–661.

Shimada, M., Han, B., Okuyama, K. and Otani, Y. (2002). Bipolar Charging of Aerosol Nanoparticles by a Soft X-ray Photoionizer. *J. Chem. Eng. Jpn.* 35: 786–793.

Wood, D.M. (1981). Classical Size Dependence of the Work Function of Small Metallic Particles. *Phys. Rev. Lett.* 46: 749.

Received for review, July 21, 2011
Accepted, October 11, 2011